tion of such surface defects in rail steels would prove invaluable in assessments of cyclic life.

(5) *Microstructure of the Weld Metal*

As only one weld metal was examined and tested in the present work, a number of selected welds in rail steel need to be studied to establish whether this particular weld metal is typical or not.

In view of the above limitations, it must be stated that the prediction of failure of the weld metal during service represents a compounded 'worst case' situation that could be ultra-conservative in nature. More reliable (experimentally determined) data are required before a justifiably realistic assessment can be achieved.

Conclusions

The work on the growth of fatigue cracks showed that

(a) the growth rates in the deformed rail steel were slightly higher than those in the undeformed rail steel, and
(b) the growth rates in the weld metal were appreciably faster and exhibited plateaux that were beyond the upper bound for rail steels.

Essentially, the cyclic-life curves show that no fatigue failures will occur during 8 years of service in both the deformed and the undeformed rail steels examined.

PART 2: METALLOGRAPHIC AND FRACTOGRAPHIC DETAILS

A section from the broken half of each fatigue fracture described in Part 1 was cut and cleaned electrolytically by use of the Endox-based technique. Each companion fracture surface was mounted in an electrically conducting medium so that the fatigue crack–microstructure profile could be studied. All the fractographic studies and most of the metallographic surveys were conducted on a Hitatchi 620 scanning electron microscope (SEM).

Measurements of the pearlite interlamellar spacing were taken for both the rail steels and the weld metal. For each microstructure, 100 random fields were taken, at a magnification of 2000 to 5000, and the number of lamellar intercepts was counted on a linear grid mounted on the screen of the SEM. The total length of line divided by the number of cementite lamellae intersected is defined as $\bar{\ell}$, the mean intercept spacing. The mean true pearlite spacing is given by $\lambda_0 = \bar{\ell}/2$. More exact forms of this equation have been developed for situations where not all the cementite platelets have a planar orientation, and details of the various methods available for the measurement of pearlite interlamellar spacing have been reported by Underwood[10].

Experimental Results

Microstructural Details

Microstructural details of the rail steel (the microstructures of the undeformed and deformed rail steel were almost identical) and of the weld metal are shown in Fig. 8. The rail steel exhibits a fine fully pearlitic microstructure, colony size approximately 50 μm, with little evidence of pro-eutectoid ferrite, while the weld metal shows extensive ferrite formation, which tends to decorate prior austenite grain boundaries. Much of the ferrite is nucleated along columnar grain boundaries (Fig. 8b) that were 0,5 to 1 mm in width. Again, the microstructure was predominantly pearlitic, and the pearlite colony was much coarser than that of the rail steel, measuring up to 300 μm in some instances. Mean measurements of true interlamellar pearlite spacing were recorded for each microstructure, with the following results: undeformed rail steel 184 nm, deformed rail steel 175 nm, and weld metal 136 nm.

Details of the nature of the pro-eutectoid ferrite formed in the weld metal are shown in Fig. 9: (a) illustrates the

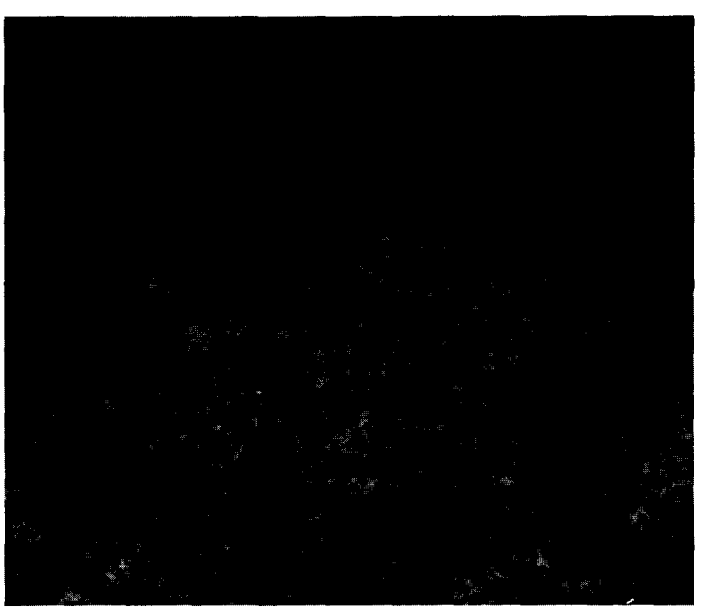

(a) General macrograph of undeformed rail steel, showing the relatively fine size of the pearlite colony and no evidence of grain-boundary polygonal ferrite

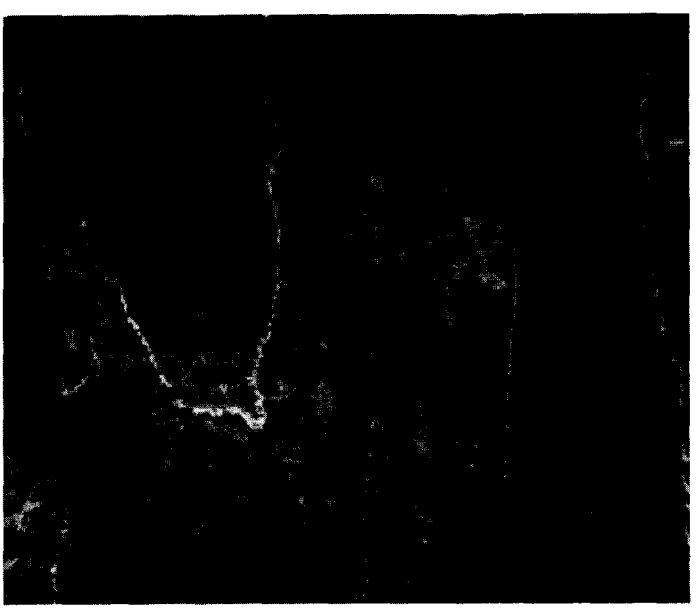

(b) General macrograph of the weld metal, showing large columnar grains decorated with polygonal ferrite, the grains varying in width from 0,5 to 1 mm; and showing the large size of the pearlite colony

Fig. 8—Microstructural details of the rail steel and the weld metal

(a) Details of polygonal ferrite along a prior austenite grain boundary

(b) Acicular nature of the grain-boundary ferrite, which could be either Widman–Statten or bainitic in nature

(c) Details of polygonal ferrite along a prior austenite grain-boundary triple point

Fig. 9—Details of pro-eutectoid ferrite in the weld metal

formation of blocky polygonal ferrite along a prior austenite grain boundary; (b) shows the acicular nature of grain-broundary nucleated ferrite, the ferrite being in the form of fine needles that grow into the pearlite and would be termed Widman-Statten ferrite, or even in the form of the inter-ferrite laths that are prevalent in upper bainitic microstructures; (c) shows the nature of the pearlite, together with polygonal ferrite formation along a prior austenite grain boundary triple point.

Detailed micrographs of the pearlite formed in the rail steel and weld metal are shown in Fig. 10. In keeping with the recorded mean measurements of the true interlamellar spacing, the weld-metal pearlite appeared generally finer than the rail-steel pearlite.

Profile of the Fatigue Cracks

The fatigue cracks in the rail steels occurred by ductile striated growth in a transgranular manner through pearlite colonies fracturing the cementite lamellae. The principal crack paths in the lamellar pearlite microstructures were along ferrite–cementite interfaces and, in a few isolated cases, along prior austenite grain boundaries. These observations are similar to those recorded by Taylor *et al.*[11]. At K_{max} values greater than 40 MPa$\sqrt{m}$, small isolated flat areas, 50 to 150 μm in size, were observed to appear in the crack profile of both the rail steels. These were shown to be isolated regions of transgranular cleavage fracture, i.e. microcleavage facets.

The profile details of the cracks in the weld-metal structures were markedly different inasmuch as the crack growth followed a rather tortuous path and exhibited large flat regions, that in some cases were up to 600 μm in length. These flat regions were indeed large transgranular cleavage facets, and the majority of the profiles

(a) Detailed view of pearlite in the microstructure of the rail steel, showing the inherent directional nature of the cementite lamellae

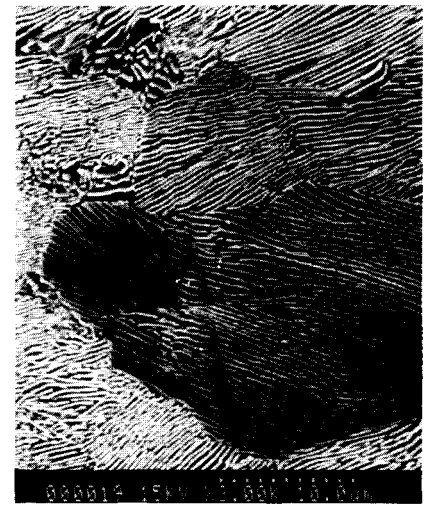

(b) Details of pearlite and ferrite formed in the weld metal, some individual pearlite colonies being only 10 μm in diameter

Fig. 10—Detailed views of the nature of the pearlite formed in the microstructures of the rail steel and the weld metal

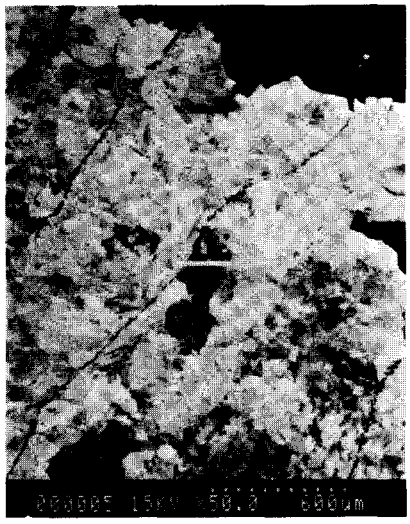

(a) Details of the fatigue region and columnar-grain growth, the flat regions on the crack profile representing transgranular cleavage facets

(b) Detailed view of (a), showing that, within the columnar grain, 300 to 600 μm in width, there are about four flat regions of fracture, i.e. four cleavage facets; thus, the size of the cleavage facet is not dictated by these coarse columnar grains but by some other microstructural unit

(c) Details of secondary cracking

Fig. 11—Profiles of fatigue cracks in the weld metal

exhibited this type of fracture mode. Details of the fatigue-crack profiles in the weld metal are shown in Fig. 11. The rough nature of the crack extension is noteworthy, as is the size of these flat transgranular cleavage regions, which were somewhat smaller than the width of the columnar grains, Fig. 11(b). Details of much secondary cracking, Fig. 11(c), were evident.

A detailed study of these flat transgranular cleavage facets showed that in many cases (Fig. 12) the fracture event occurred along and within the grain-boundary regions of pro-eutectoid ferrite.

Many instances of isolated crack formation were recorded (Fig. 13) in the microstructure of the weld metal in regions that were some distance from the main fatigue crack. Instances of cracking along prior austenite grain boundaries, Fig. 13(a), and at non-metallic inclusions, Fig. 13(c), were also evident.

Fractography

The general nature of the fatigue cracks in rail steels at the initial stages of testing are shown in Fig. 14. From this it can be seen that the failure mode is by transgranular ductile striated growth. This growth shows marked directionality effects, which probably result from the growth of fatigue cracks through adjacent pearlite colonies with different orientations. Such striations do not reflect the pearlite lamellar structure.

At K_{max} values approaching 40 MPa$\sqrt{m}$, the onset of isolated regions of transgranular cleavage facets occurred in both the deformed and the undeformed rail steel, and details of these facets are shown in Fig. 15. The size of these individual cleavage facets was 50 to 100 μm. Initiation points for each facet were clearly in evidence, and growth generally emanated in the direction of macrocrack growth. Also, these isolated facets occurred mainly at the centre of the specimens. Similar observations have been made by other workers[12]. This means that the critical strain for fracture is first satisfied at the centre of the crack envelope and, as the crack continues to grow, cleavage facets occur in groups across the whole crack front.

The following features are typical of these cleavage facets.

(1) They are fan-shaped in nature and have a definite initiation point. There is no evidence that cleavage initiates from a cracked cementite lamella, but a few instances of facets initiated from inclusions were recorded.
(2) Lines run outwards from the initiation site like the ribs of a fan.
(3) The usual morphology is fan-shaped, the edge opposite the initiation site being semi-circular in shape.

At K_{max} levels approaching an approximate K_Q of 50 MPa$\sqrt{m}$, the K value at which fast fracture occurs, the predominant fracture mode is cleavage, and an indication of the extent of cleavage-facet formation is shown in Fig. 16.

The incidence of facet formation with increasing K_{max} in the deformed and undeformed rail steels is portrayed in Fig. 17. Essentially, the critical K_{max} value for the initial formation of cleavage facets is 35 and 37 MPa$\sqrt{m}$ for the deformed and the undeformed rail steel respectively. With increasing K_{max} the incidence increases until fast failure occurs at a K_{max} of 50 MPa$\sqrt{m}$, i.e. when K_Q is attained.

Unlike the microstructures of the rail steel that exhibited the initiation and gradual increase in cleavage facets with increasing length of fatigue crack, the microstructure of the weld metal exhibited predominantly large cleavage facets even at the start of fatigue testing. Fractographic details are shown in Figs. 18 and 19. In

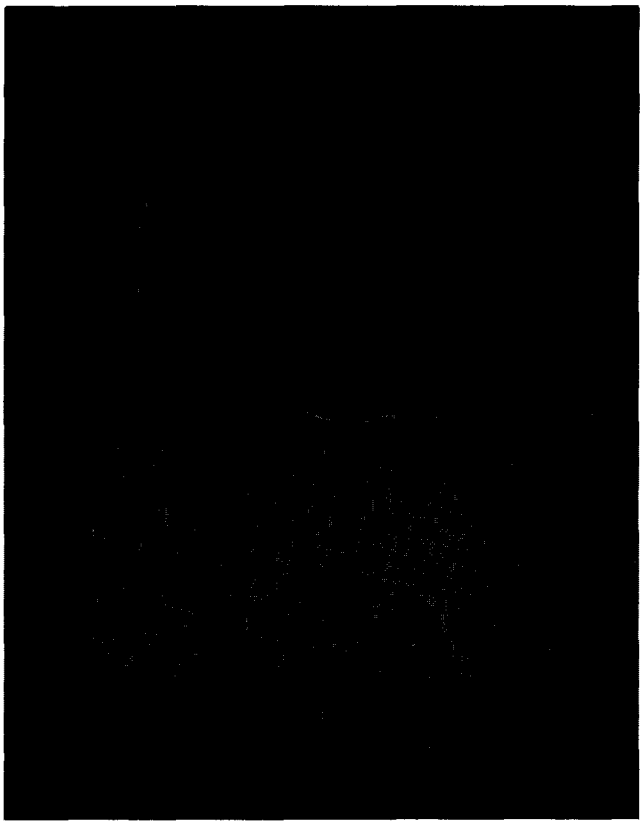

(a) The fatigue crack has propagated through a region of grain-boundary ferrite, and then the main crack front suddenly changed direction and propagated through a pearlite colony, leaving a secondary crack in the grain-boundary ferrite

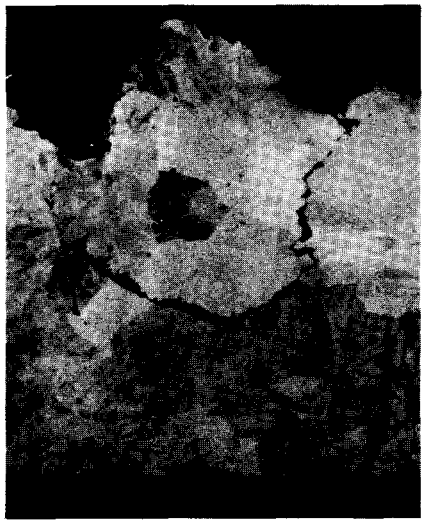

(b) Much of the crack growth is along grain boundaries decorated with pro-eutectoid ferrite, the size of the pearlite colony being about 100 μm

Fig. 12—Crack profiles showing the propagation of fatigue cracks along grain-boundary ferrite regions in the weld metal

(a) An isolated secondary crack 50 μm in length, probably along a prior austenite-grain boundary

(b) An extensive secondary crack some 4 mm away from the main fatigue-crack front

(c) Evidence of secondary cracks initiating from a type I manganese sulphide inclusion

Fig. 13—Details of secondary cracks in the weld metal at regions somewhat remote from the main fatigue-crack front

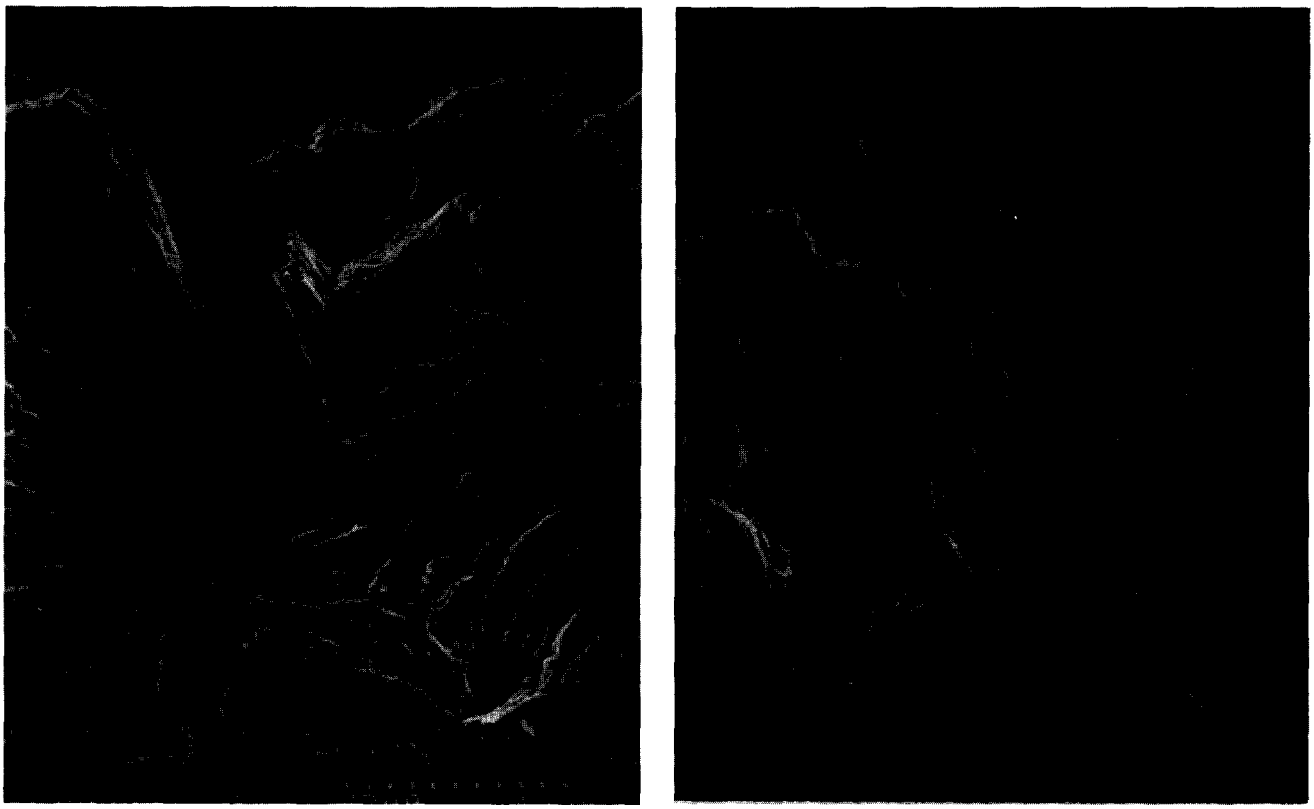

(a) → Direction of crack growth in undeformed rail steel

(b) → Direction of crack growth in deformed rail steel

Fig. 14—Fractographic details of fatigue cracks in the rail steel at ΔK levels of about 20 MPa$\sqrt{m}$, showing that the cracks are extended by ductile striated growth that has an extensive, high degree of directionality; such directionality probably results from fatigue-crack growth following the orientation of the pearlite colonies

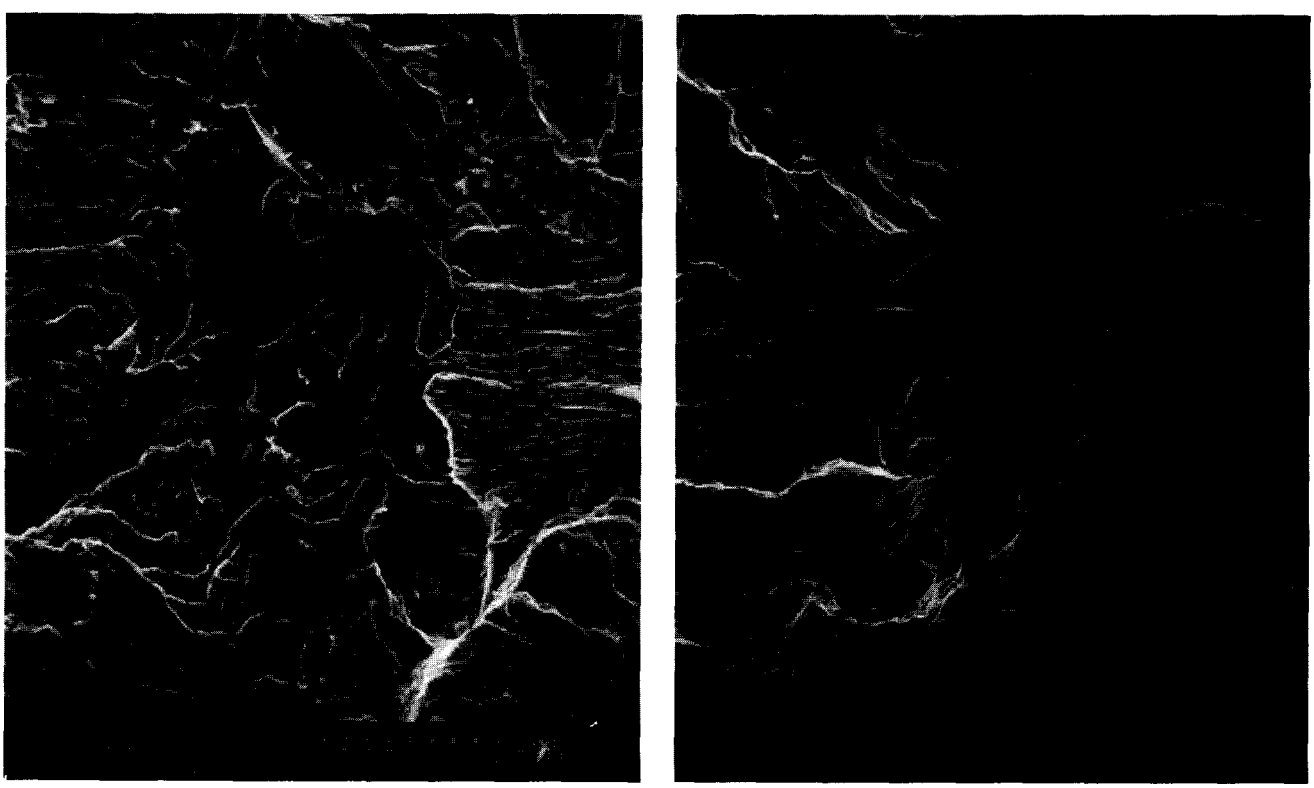

(a) Isolated cleavage facet 50 μm in length (tilt angle 0°)

(b) Isolated cleavage facet (tilt angle 40°)

Fig. 15—Isolated incidences of transgranular cleavage facets formed in the undeformed rail steel at K_{max} values of about 40 MPa$\sqrt{m}$

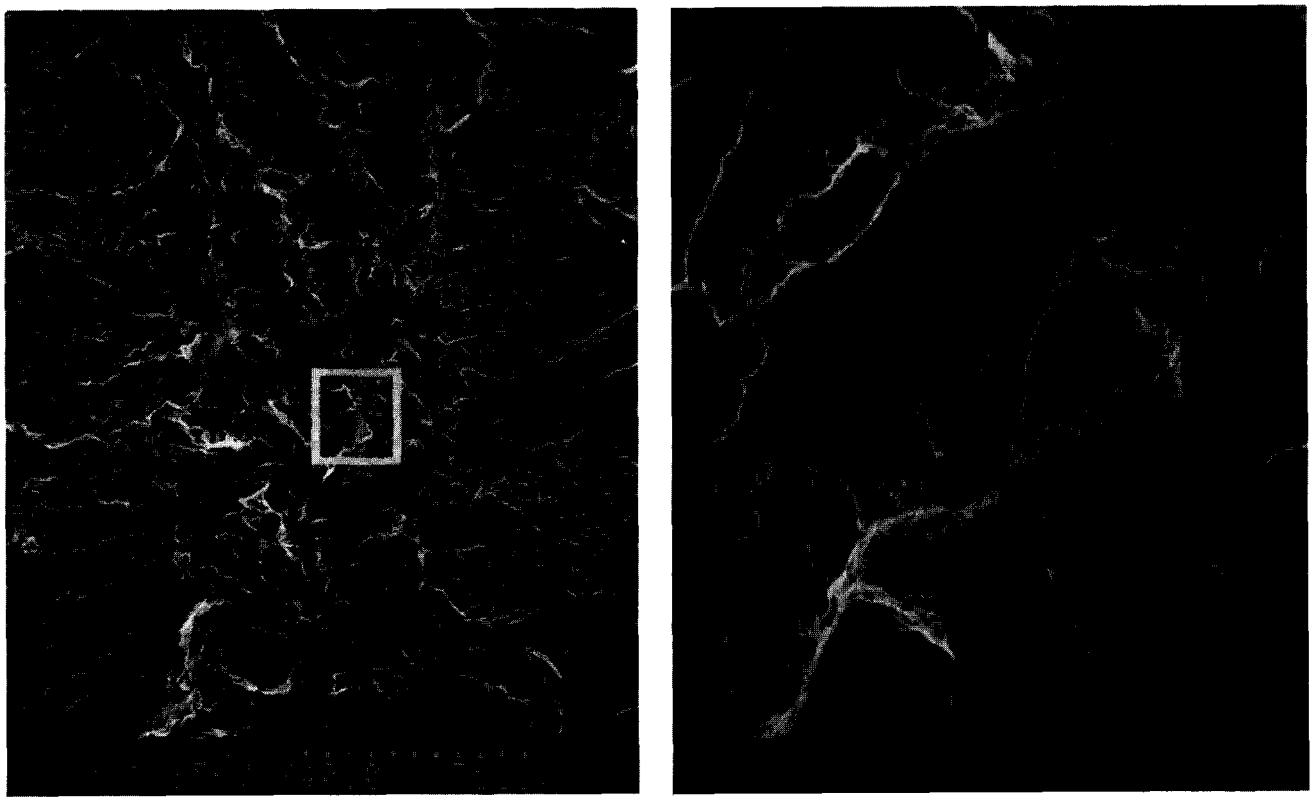

(a) General details of the extent of cleavage-facet formation at a K_{max} value approaching fast fracture

(b) Detailed view of the cleavage facets formed in (a), showing the size of the facets to be about 50 to 100 μm

Fig. 16—Details of cleavage facets in the deformed rail steel

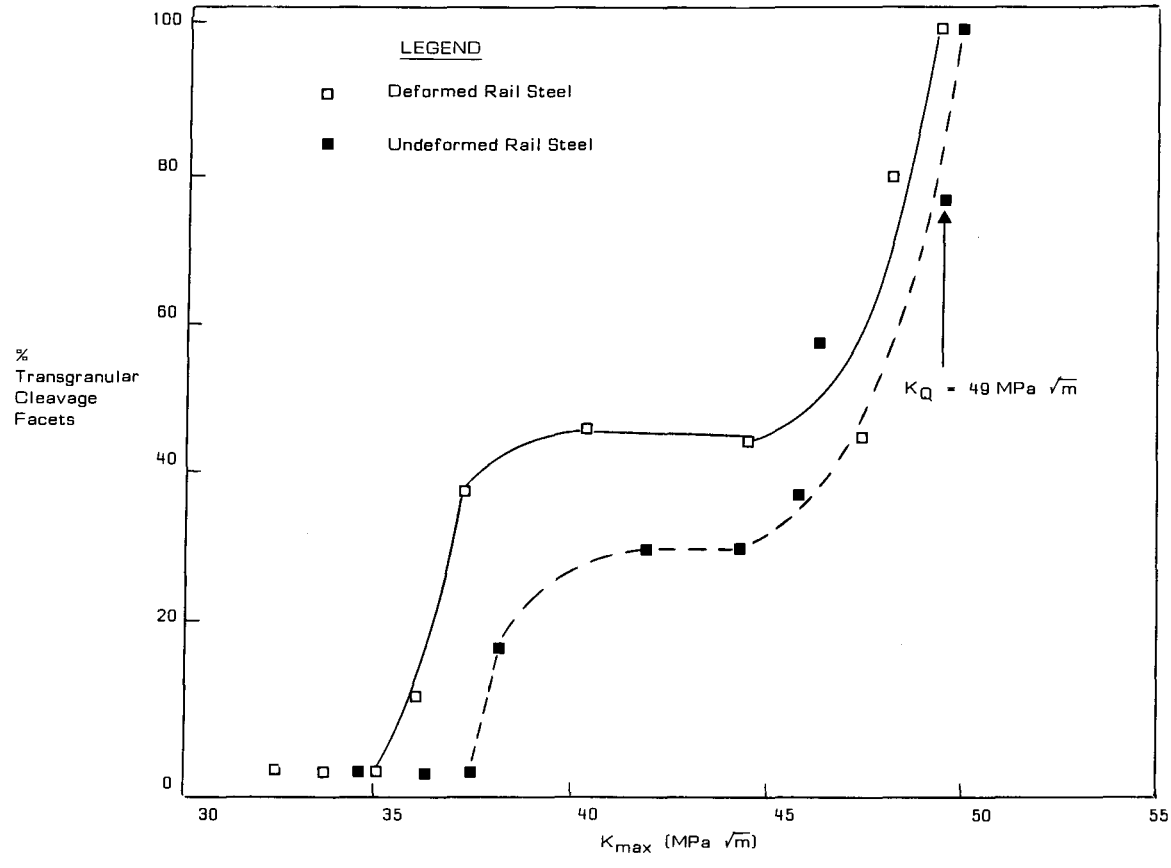

Fig. 17—Effect of K_{max} on the incidence of cleavage facets in the deformed and undeformed rail steel

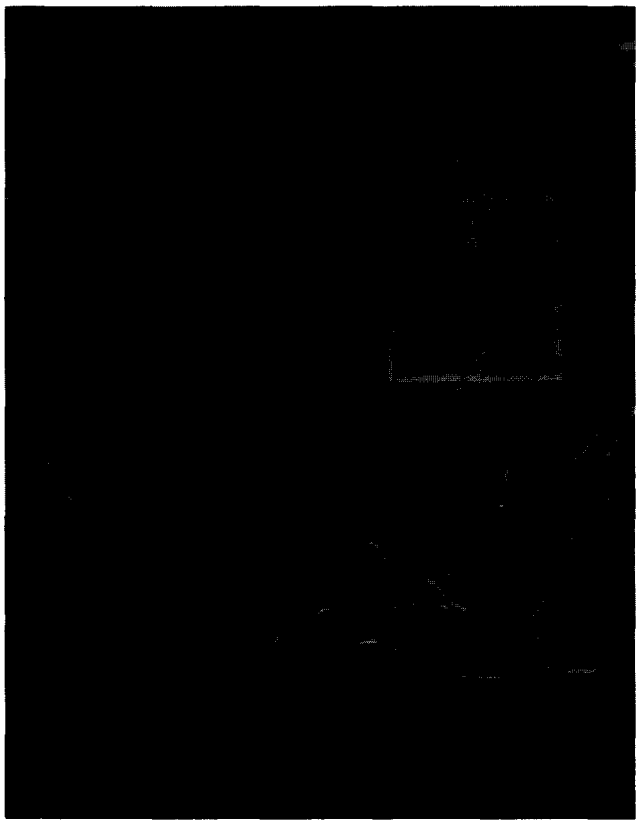

(a) Some large cleavage facets, about 500 μm in size, showing a ribbon of ductile striated cracks (boxed region)

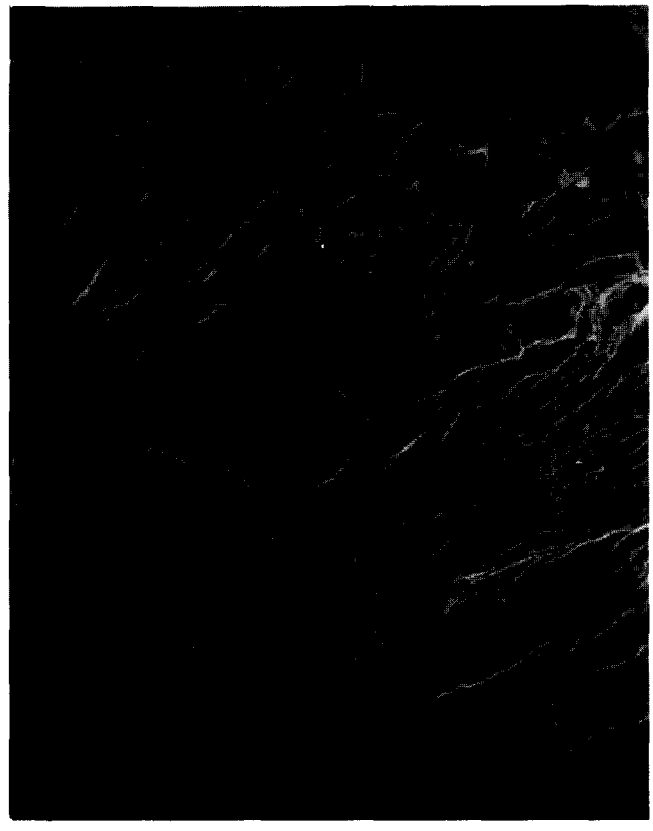

(b) Detailed view of the boxed region in (a), showing the ribbon of ductile striated cracks 60 μm thick surrounded by cleavage facets

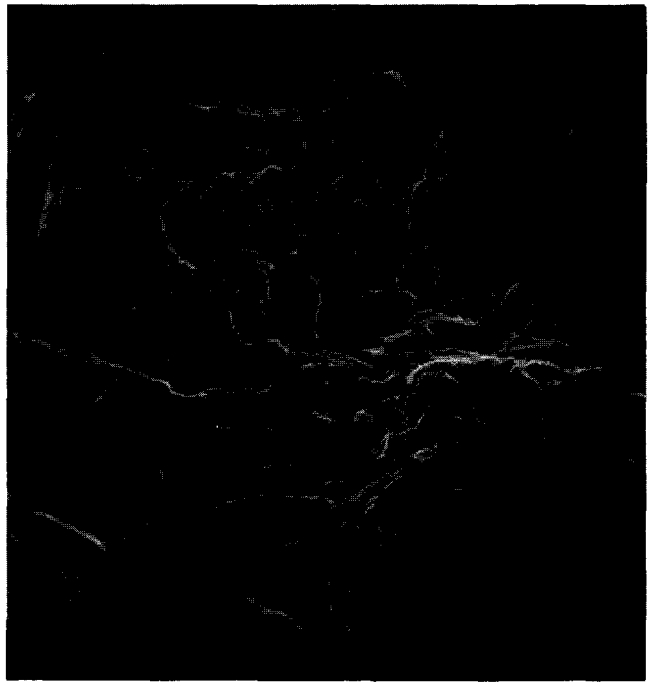

(c) Region where the fatigue cracks was extended predominantly by ductile striated growth (cleavage region outlined by black broken line)

Fig. 18—Fractography of the region of fatigue-crack growth in the weld metal

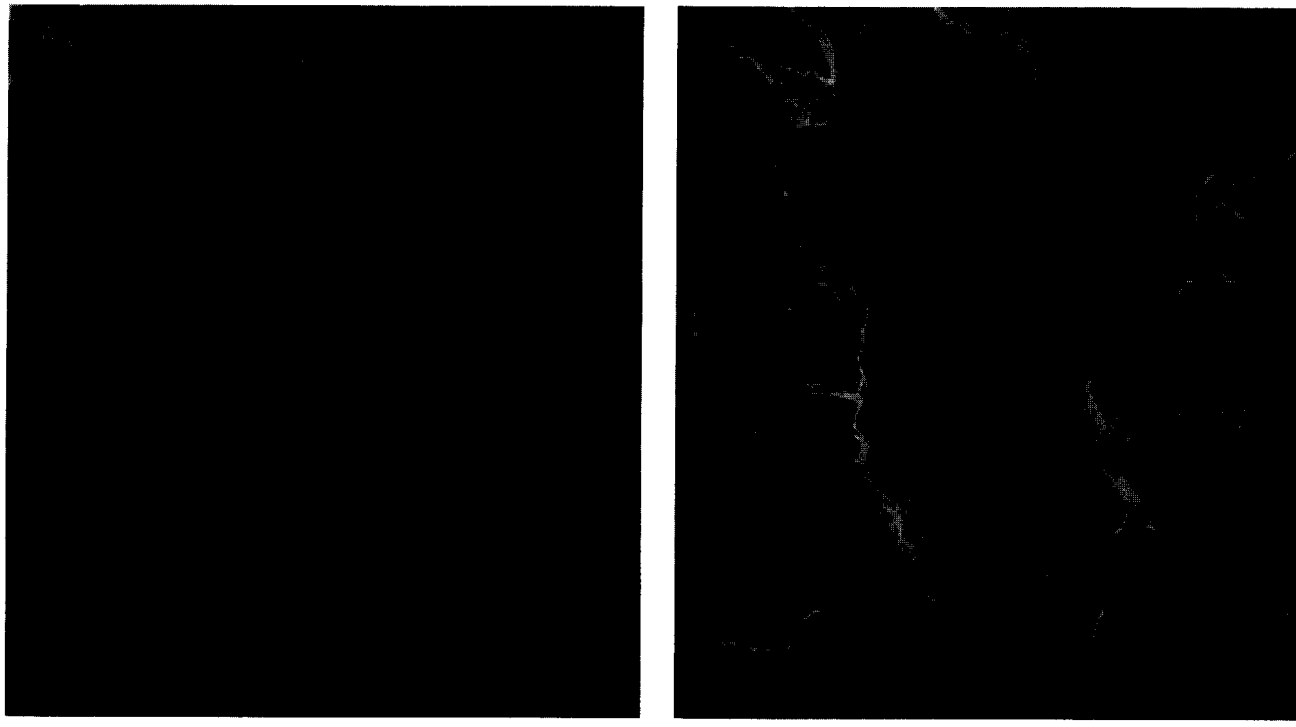

(a) (b)

Fig. 19—Details of transgranular cleavage facets in the weld metal, showing the secondary crack in the austenite-grain boundary (a); this is probably due to the presence of grain-boundary polygonal ferrite that preferentially harbours cracking in the weld metal; again, the cleavage facet is about 500 μm in diameter

some regions, large cleavage facets, up to 600 m in size, were connected by thin ribbons of material that had failed by ductile striated fatigue-crack growth, Figs. 18(a) and (b), while in a few isolated cases the dominant fracture mode was ductile striated growth, Fig. 18(c). Details of the nature of the large cleavage facets are illustrated in Fig. 19, which shows in (a) the occurrence of secondary cracking along a prior austenite grain boundary. This probably results from the presence of grain-boundary pro-eutectoid ferrite, which preferentially harbours cracking in weld metal (Fig. 12).

Discussion

The formation of isolated transgranular cleavage facets during fatigue at a critical K_{max} level and their subsequent increasing incidence with increasing K_{max} level have been observed in steel by other investigators[6,12–14]. Aita and Weertman[12] observed that, in pearlitic microstructures, the size of the cleavage facet formed during fatigue was related to the size of the pearlite nodule, and was independent of both the size of the pearlite colony and the size of the prior austenite grains. A pearlite colony is an area within which the carbide lamellae have the same orientation, whereas a pearlite nodule is a cluster of wedge-shaped pearlite colonies that emanate from a nodule core, and this is shown schematically in Fig. 20. In the microstructure studies of the rail steel, the size of the pearlite colony was found to vary from 20 to 50 μm, while the size of the prior austenite grains could not be easily assessed. Also, the size of the pearlite nodules was not easy to determine but, in the few cases where definite nodule formation was evident, their size was 60 to 100 μm. This particular size agrees well with the dimensions of the initial isolated cleavage facets observed at K_{max} levels of 40 MPa$\sqrt{m}$, viz 40 to 100 μm, and hence tends to confirm the observations of Aita and Weetman that the structural parameter controlling cleavage fracture in fully pearlitic microstructures is the size of the pearlite nodules.

The onset of cleavage-facet formation occurs if a critical tensile stress, σ_{yy}, sufficient to cause cleavage propagation from a crack in carbide lamellae is attained

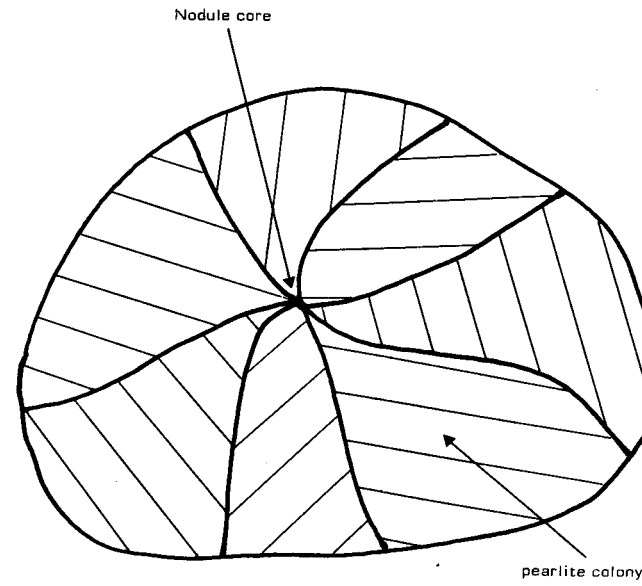

Fig. 20—Schematic representation of a pearlite nodule

at some characteristic distance as being the size of two pearlite nodules, i.e. 160 μm; using σ_y = 570 MPa and a critical K value = 35 MPa$\sqrt{m}$, a value of 1600 MPa was calculated for σ_{yy}. This value for the critical tensile stress ahead of the crack tip to initiate cleavage facets agrees well with the values calculated by Richie and Knott (σ_{yy} = 1300 MPa) for low-carbon steels[15], with the various values of cleavage stress reported by Hahn[16], and with the recently reported[17] cleavage-fracture stress values in a fully pearlitic steel of 1600 to 1900 MPa$\sqrt{m}$. With increasing K_{max} level, both the deformed and the undeformed rail steels exhibited an increase in the amount of cleavage until K_{max} is about 50 MPa, at which fast failure occurs.

The deformed and undeformed rail steels exhibited initial cleavage-facet formation at K values of 35 and 37 MPa$\sqrt{m}$ respectively, and between K levels of 35 and 45 MPa$\sqrt{m}$ the deformed steel exhibited measurably more cleavage facets on the fatigue surface (Fig. 17). These trends are probably due to the effect of deformation on the flow properties of the rail steel.

The microstructure of the weld metal exhibited long columnar grains, 300 to 600 μm in width, the grain boundaries being decorated with pro-eutectoid ferrite. Such grain growth results from the rapid cooling conditions that were prevalent in the weld metal owing to the presence of large heat sinks (i.e. rails) on either side of the weld. The grain size of the prior austenite was about 200 μm, and the size of the pearlite colonies varied between 20 and 120 μm. The size of the pearlite nodules in this particular microstructure could not be assessed reliably.

The cleavage facets, which were the dominant fracture node at all ΔK levels of fatigue testing, varied in size from 150 to 600 μm, and were in some cases connected by ribbons of ductile striated regions of fatigue cracks. Thus, in the weld-metal microstructures, there was no clear indication of the nature of the structural parameter controlling the mode of cleavage fracture. Another general observation was that the fracture path tended to lie in regions of pro-eutectoid ferrite and, as such regions occurred along austenite grain boundaries (generally 200 μm in size) and columnar grain boundaries (300 to 600 μm in width), this may explain the large variation in the size of the cleavage facets.

Although the microstructure of the weld metal was coarse, the mean measurements of the true interlamellar spacing showed that the pearlite in the weld metal was measurably finer than that in the rail steels. Such differences can be explained in terms of the cooling rate through the pearlite transformation, the weld metal being subjected to rapid cooling through the transformation while the rail steels are normalized and hence had been subjected to slower air cooling rates.

Summary and Conclusions

In the rail steels at initial ΔK levels, the fatigue fracture mode was ductile striated growth. At K_{max} levels approaching 35 MPa$\sqrt{m}$, cleavage facets were observed on the surface of fatigue cracks, the incidence of which increased with K_{max} until final fast failure occurred, at a K_{max} value of about 50 MPa$\sqrt{m}$. The fatigue-fracture surface in the deformed rail steel exhibited cleavage facets at a slightly lower K_{max} value, and contained more cleavage facets at a given K_{max} value, than the undeformed rail steel. The size of the cleavage facets in the rail steels agreed well with the dimensions of the pearlite nodules—60 to 100 μm.

The weld metal had a coarser microstructure and contained large columnar grains, 300 to 600 μm in width. Cleavage failure was the dominant fracture mode at all the ΔK levels of fatigue testing, the size of the cleavage facets varying widely from 150 to 600 μm. Regions of ductile striated fatigue cracks were evident within the dominant cleavage failure mode. The large variation in cleavage-facet size in the weld metal may be explained by the following facts.

(a) The cracks were propagated generally in regions of pro-eutectoid ferrite.
(b) The pro-eutectoid ferrite was nucleated both at some prior austenite grain boundaries and along the coarse columnar grains.

Differences in cooling rate through the pearlite transformation resulted in the weld metal having a finer mean true interlamellar pearlite spacing than the rail steels.

Failures were predicted in the weld metal, but it must be realized that all the input parameters represented 'worst case' situations and, as such, the predictions could well be ultra-conservative.

ACKNOWLEDGEMENTS

The author thanks Professors G.G. Garrett and A. Kemp for their helpful discussions, and Mr A.M. Bissell, Babcock Power Ltd, Renfrew, Scotland, for his assistance in the fractographic study.

References

1. GARRETT, G.G., and TAIT, R.B. A fracture mechanics assessment of the significance of surface defects in chrome manganese rails at Richards Bay Coal Terminal, 16th May, 1983.
2. KEMP, A. University of the Witwatersrand, private communication, 1985.
3. HILL, S.J., and BOOTLE, N.F. *Fracture 1977,* Waterloo (Canada), vol. 2, ICF4, p. 1233.
4. STEELE, R.K. *Maters. Evol.,* Oct. 1980. p. 33.
5. EVANS, P.R.U., *et al. J.I.S.I.,* Jun. 1970. p. 560.
6. BEEVERS, C.J., COOKE, R.J., KNOTT, J.F., and RITCHIE, R.O. *Metal Sci.,* vol. 9. 1975. p. 119.
7. IRMIN, G.R., *et al. Report* NRL-5698. Nov. 1967.
8. VISHNEVSKY, C., and STEIGERWALD, E.A. *Report CR* 68-09(F). Watertown (U.S.A.), Army Materials and Mechanics Research Centre, Nov. 1968.
9. WESSEL, E.T., *et al. Report* DDC-AD801001. 1966.
10. UNDERWOOD, E.E. Quantitative stereology. Addison-Wesley, 1970. p. 73.
11. TAYLOR, J.G., NARIN, P.E., and WATSON, P. *Fracture 1977.* Waterloo (Canada), vol. 2, ICF4, p. 681.
12. AITA, C.R., and WEERTMAN, J. *Script. Metall.,* vol. 12. 1978. p. 837.
13. HEALD, P.T., LINDLEY, T.C., and RICHARDS, C.E. *Mats. Sci. Engng,* vol. 10. 1972. p. 235.
14. BULLOCH, J.H. Ph.D. Thesis, Strathclyde University, 1980.
15. RITCHIE, R.O., and KNOTT, J.F. *Mats. Sci. Engng,* vol. 14. 1975. p. 8.
16. HAHN, G.T. *Metall. Trans.,* vol. 15A. 1984. p. 947.
17. LEWANDOWSKI, J.J., and THOMPSON, A.W. *6th International Conference on Fracture.* New Delhi, 1984. vol. 2, p. 1515.